4th Hinode *Science Meeting: Unsolved Problems and Recent Insights*
ASP Conference Series, Vol. 455
L. R. Bellot Rubio, F. Reale, and M. Carlsson, eds.

Detection of Vortex Tubes in Solar Granulation from Observations with SUNRISE

O. Steiner,[1] M. Franz,[1] N. Bello González,[1] Ch. Nutto,[1] R. Rezaei,[1]
V. Martínez Pillet,[2] J. A. Bonet,[2] J. C. del Toro Iniesta,[3] V. Domingo,[4]
S. K. Solanki,[5,6] M. Knölker,[7] W. Schmidt,[1] P. Barthol,[5] and A. Gandorfer[5]

[1]*Kiepenheuer-Institut für Sonnenphysik, Schöneckstrasse 6, 79104 Freiburg, Germany*

[2]*Instituto de Astrofísica de Canarias, C/Vía Láctea s/n, 38200 La Laguna, Tenerife, Spain*

[3]*Instituto de Astrofísica de Andalucía (CSIC), Apdo. de Correos 3004, 18080 Granada, Spain*

[4]*Grupo de Astronomía y Ciencias del Espacio, Universidad de Valencia, 46980 Paterna, Valencia, Spain*

[5]*Max-Planck-Institut für Sonnensystemforschung, 37191 Katlenburg-Lindau, Germany*

[6]*School of Space Research, Kyung Hee University, Yongin, Gyeonggi 446-701, Republic of Korea*

[7]*High Altitude Observatory, National Center for Atmospheric Research (NCAR), Boulder, CO 80307-3000, USA*

Abstract. We investigated a time series of continuum intensity maps and Dopplergrams of granulation in a very quiet solar region at the disk center, recorded with the Imaging Magnetograph eXperiment (IMaX) on board the balloon-borne solar observatory SUNRISE. We find that granules frequently show substructure in the form of lanes composed of a leading bright rim and a trailing dark edge, which move together from the boundary of a granule into the granule itself. We find strikingly similar events in synthesized intensity maps from an ab initio numerical simulation of solar surface convection. We conclude that these *granular lanes* are the visible signature of (horizontally oriented) vortex tubes. The characteristic optical appearance of vortex tubes at the solar surface is explained. This paper is a summary and update of the results previously presented in Steiner et al. (2010).

1. Introduction

Solar granulation is the superficial, visible manifestation of the motion of plasma in the convection zone of the Sun. Warm plasma ascends to the solar surface within granules, cools radiatively at the surface, and returns back into the convection zone within the intergranular lanes. The difference in temperature between the warm ascending and the cool descending plasma accounts for the observed intensity contrast between the bright

granules and the network of dark intergranular lanes, and for the convective blueshift, the limb effect, and the C-shape of photospheric spectral lines (Stix 2002).

Thus, the concept of an "average granule" was developed with a mean velocity field and mean values for lifetime and effective diameter (see Stix 2002, and references therein). Although fundamentally correct, this picture of quasi-laminar flow cannot account for the fine structure of granulation, which has become apparent through observations with the balloon-borne solar observatory SUNRISE (Barthol et al. 2011; Solanki et al. 2010). Frequently occurring fine structure elements are *granular lanes*, typically consisting of a bright and a dark edge, which travel from the visible boundary of granules into the granule itself. In the following, we present several events in maps of the continuum intensity and the corresponding Dopplergram. We reveal their physical nature with the help of numerical simulations as the visible signature of vortex tubes. This paper is a summary and update of the results previously presented in Steiner et al. (2010).

2. Observation and Data Reduction

The observational data were obtained on June 9, 2009 from 00:35:49 UT to 02:02:48 UT with the Imaging Magnetograph eXperiment (IMaX), on board SUNRISE. For a detailed description of the IMaX instrument and the data reduction procedure, we refer to Martínez Pillet et al. (2011). Images were taken for four polarimetric states with the etalon being centered at the wavelength positions ±80, ±40, and +227 mÅ with respect to the core of the Fe I spectral line at 5250.2 Å. The continuum images have an effective exposure time of 6 s. All images were reconstructed using deconvolution with a point spread function (PSF) and Wiener-Helstrom filtering. The PSF was obtained from phase diversity image pairs taken close in time to the measurements. We obtained two consecutive series of science images that together cover a time period of 53.9 minutes with a cadence of 33 s. The noise level is 10^{-3} of the continuum intensity for the non-reconstructed and $(2.5-3)\times 10^{-3}$ for the reconstructed data. A spatial resolution of 0.″15–0.″18 in all Stokes parameters was achieved by combining the onboard image stabilization system (Berkefeld et al. 2011) with the phase-diversity-based post-processing technique. These data show granulation of a very quiet solar region in a field of view (FOV) of approximately 51.″5 × 51.″5 at the disk center. The Doppler velocity, v_D, is inferred from a Gaussian fit to the intensities at the four wavelength points in the spectral line, after normalization to the local continuum. In addition, a spatially dependent blueshift over the FOV was taken into account in the course of the fit procedure. The zero point of the velocity corresponds to the mean wavelength position over the full FOV, corrected for a convective blueshift of 0.2 km s^{-1}. We estimate the absolute error of v_D to be about ±0.2 km s^{-1}.

3. Fine Structure Elements of Granules

Figure 1 shows the time sequence of the formation and evolution of the type of granular fine structure that we consider in this paper. The top row shows the non-reconstructed intensity maps, the second row the corresponding reconstructed images. From this sequence, one can see the following: the granule in the center of the images around $(x, y) = (2.5, 2.5)$ Mm expands rapidly, apparently colliding with the two neighboring

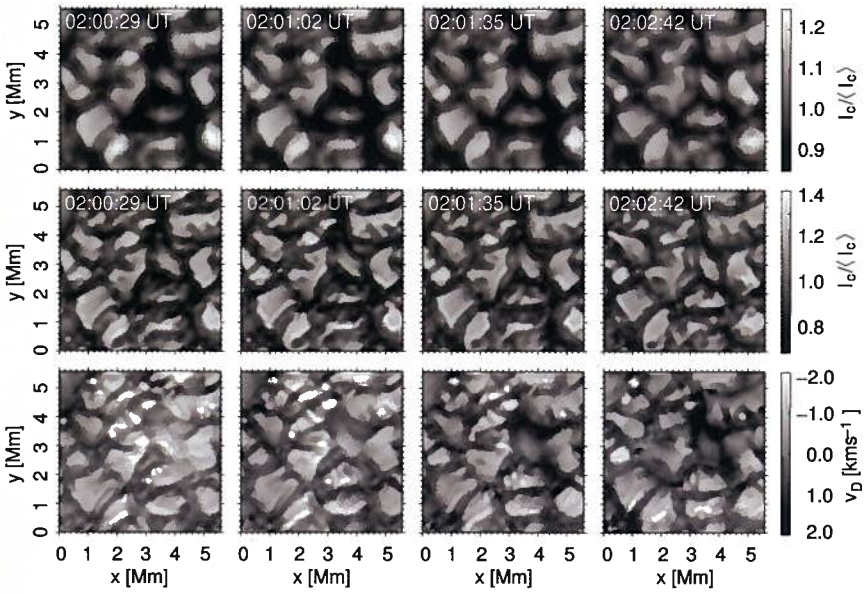

Figure 1. Time series showing the development of a bright/dark granular lane at the right boundary of the granule in the image center at $(x, y) = (2.5, 2.5)$ Mm. *Top:* sequence of non-reconstructed images in the continuum intensity at $\lambda = 5250.4$ Å. *Middle:* corresponding sequence of reconstructed images. *Bottom:* corresponding sequence of Doppler maps. The maps are small subfields of the full FOV, measuring 5.6×5.6 Mm each. Positive velocities correspond to downdrafts.

granules on the right hand side. At time t = 02:00:29 UT, the right border of the expanding granule starts to become slightly enhanced in intensity at $(x, y) = (2.8, 2.7)$ Mm. In the next frame—33 s later—a bright rim detaches from the border of the granule and moves into the granule itself. The ends of the bright lane, however, remain attached to the granule border. At t = 02:01:35 UT, a second rim, similar in brightness, develops in the upper right side of the granule, connecting to the existing one at $(x, y) = (2.8, 2.9)$ Mm, and complementing it to a Y-shaped bright lane. In the course of this development, a dark lane immediately adjacent but trailing the bright lane appears, giving the impression of a sharp edge to the trailing side of the bright lane. This sequence of events is visible in both the non-reconstructed and the reconstructed images and is therefore not an artifact of the reconstruction. The observing sequence stops at 02:02:42 UT. Typically, such bright/dark *granular lanes* either retreat back to the boundary of the granule or disappear with the subsequent dissolution of the granule. They should not be mistaken with the dark intergranular lanes.

The sharp separation of the right boundary region from the rest of the granule by the granular lane is less pronounced in the Doppler maps (the bottom row of Fig. 1), where the granule appears undivided and still intact. The granular lane is visible only at the beginning of the sequence but is barely noticeable at times later than t = 02:02:09 UT. The bright lane and the area to the left (ahead) of it show flows in the upward direction with speeds of up to -1.8 km s^{-1}. Most of the area behind the bright

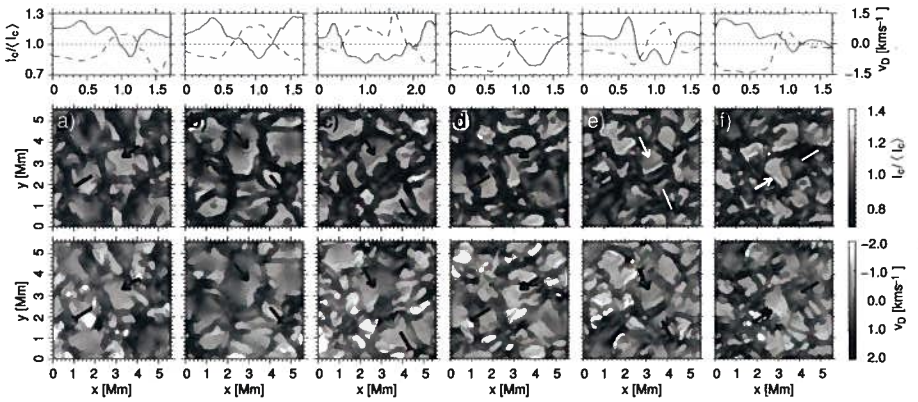

Figure 2. Instances of granular lanes. *Middle:* reconstructed images of the continuum intensity at $\lambda = 5250.4$ Å. *Bottom:* corresponding sequence of Doppler maps. *Top:* plots of the relative intensity (solid curve) and the Doppler velocity in km s^{-1} (dashed curve) in a section running from the tip of the arrow to the opposite inner end of the black mark indicated in the intensity and Doppler maps. Positive velocities represent downdrafts, distances are given in Mm.

rim, including the dark lane, harbors upflows as well. Close to the border of the granule and within the adjacent intergranular lane, the plasma flows in the downward direction with speeds of up to 1.2 km s^{-1}.

Figure 2 displays six instances of events similar to the one shown in Figure 1. The middle row shows reconstructed intensity maps; located below are the corresponding Doppler maps. The panels in the top row show plots of the intensity and the Doppler velocity along the section indicated in the maps by the black arrows and marks. The abscissa of each plot runs from the tip of the arrow to the inner end of the opposite mark.

Typically, granular lanes have an oval outline (cf. Figs. 2a-c), but straight lanes occur as well (cf. Figs. 2e-f). Some bright lanes lack their distinct dark counterpart, like in Fig. 2c, and sometimes there exists a solitary dark lane or a darkish area moving into the granule without a distinct leading bright lane (cf. Figure 2f). Sometimes the trailing dark lane starts to separate from the leading bright lane, lagging behind, as is apparent in the last image of the time sequence of Figure 1.

Flows are always in the upward direction within and ahead of the bright lane, with typical speeds of -0.8 to -1.4 km s^{-1}. Also within the trailing dark lane, there are mostly updrafts of similar speeds. The area behind the bright/dark lane shows upflows and/or downflows. The adjoining intergranular lane always shows downdrafts with typical speeds of 1.0 km s^{-1}. The edge of the bright/dark lanes moves in the horizontal direction with proper velocities between approximately 1 and 4 km s^{-1}. The observed lanes show lifetimes from 1.5 to 6.5 minutes. Within a time period of 53.9 minutes and the given FOV, we found 21 events of granular lanes, i.e., 0.017 events Mm^{-2} hr^{-1}. This number must be considered a lower limit since we picked only the most salient events.

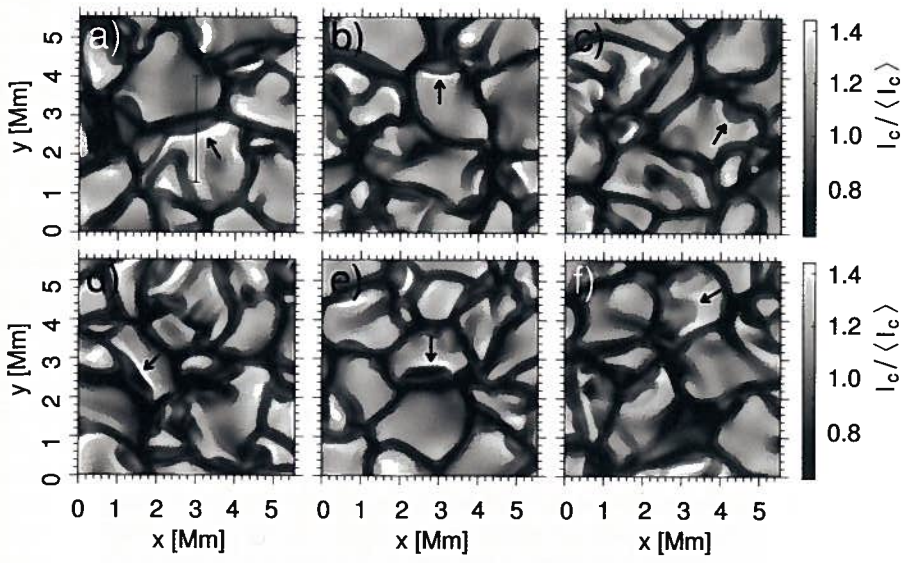

Figure 3. Instances of granular lanes (marked by arrows) from the numerical simulation. The images show the synthesized continuum intensity at 5250 Å in a subfield of 5.6 Mm × 5.6 Mm of the full simulation domain. The black line in panel a indicates the location and extension of the vertical cross section of Figure 4. From Steiner et al. (2010). Reproduced by permission of the AAS.

4. Numerical Simulation

The simulation was carried out with the CO^{5}BOLD code (Freytag et al. 2002, 2011). It solves the coupled system of the equations of compressible magnetohydrodynamics in an external gravity field and with non-local, frequency-dependent radiative transfer in three spatial dimensions. Further details of the method can be found in Schaffenberger et al. (2005, 2006).

The computational domain extends over a height range of 2.8 Mm in which the mean surface of optical depth unity is located in the middle. The horizontal extension is 9.8 Mm. The spatial resolution is 40 km in the horizontal direction, while it increases continuously in the vertical direction from 50 km in the lower part to 20 km in the middle and upper part. The simulation domain contains a weak magnetic field, which was advected by rising plumes through the bottom boundary, similar as in Steiner et al. (2008). The simulation was carried out for a real time period of 55.7 minutes from which the emergent continuum intensity at 6300 Å was synthesized with a cadence of 5 s. For the synthetic intensity maps of Fig. 3, we have computed the intensity at 5250 Å for a better comparison with the IMaX data.

Figure 3 shows subfields of synthesized intensity maps. Figure 3a shows a pair of granular lanes resembling the event shown in Figure 1. Other maps show events strikingly similar to the ones of Fig. 2, including a bright lane without trailing dark lane (Fig. 3c), an exceptionally dark, straight lane (Fig. 3e), and a darkish area moving into the granule lacking a leading bright/dark lane (Figure 3f).

We find 32 events, i.e., 0.37 events $\mathrm{Mm^{-2}\,hr^{-1}}$, which is more frequent than in the observations. Similar to the observations, the lanes move horizontally with speeds of 1–5 $\mathrm{km\,s^{-1}}$, have a lifetime of several minutes, seem to originate from collisions with neighboring granules, and sometimes retreat back to the boundary of the granule or dissolve together with the granule. The simulations show a larger variety of appearances of granular lanes than the observations do, including solitary dark lanes, ring like lanes, or the passage of a granular lane across an intergranular lane to the neighboring granule.

5. Identification with Vortex Tubes

In order to reveal the physical nature of these objects, we now study a vertical cross section through the computational domain at the location of a representative granular lane. Figure 4 is a cross section through the granular lane of Fig. 3a, at the position and of length as indicated by the black line in Figure 3a. It shows the temperature (color scale), together with the velocity projected on the plane of section (arrows), and the continuum optical depths of $\log\tau_c = -1.0$, 0.0, and 1.0 (white, horizontally running contours). The yellow/black dashed contour refers to the 7000 K isotherm. The panel on top of the cross section shows the corresponding synthesized continuum intensity at $\lambda = 5250$ Å.

From Fig. 4, it becomes immediately evident that the granular lane is caused by the vortical flow located at $(y, z) = (4.3, -0, 1)$ Mm. For all the instances of granular lanes shown in Fig. 3, and for additional 20 events, we have verified that they were all due to vortical flows similar to the one shown in Figure 4. The vorticities of these flows have a horizontal orientation and show a coherent structure over a granular scale. In the following we shall refer to these objects as *vortex tubes* according to terminology in turbulence theory.

A common property of all the vortex tubes that we have inspected is that they contain relatively cool material. As a consequence, the surface of optical depth unity is always significantly depressed at the location of the vortex tube, while the maximum depression coincides approximately with the location of the tube axis, as is the case in Figure 4. Warm plasma flowing upward must circumvent this cool material, which presents an obstacle to the general heat flow. The deviated warm material joins the upflowing side of the vortex tube, appearing at the surface where the 7000 K isotherm in Fig. 4 approaches or even surpasses the surface of $\tau_c = 1$. This configuration causes the bright lane at $y = 4.05$ Mm. Starting from this location, the isotherm drops rapidly toward the vortex tube—more steeply than the $\tau_c = 1$ surface—and causes the sharp edge between the bright lane and the adjoining dark plateau. In the particular case investigated here, no pronounced dark lane exists because the area further downstream of the vortex-tube axis stays dark (also cf. Fig. 3a) and does not show an increase in intensity as in other cases. Upstream and within the bright lane, the velocity has a significant component in the upward direction in agreement with the observations. In the range of the dark area and immediately above the vortex tube, plasma flows in a rather horizontal direction. This flow is expanding, accelerated by the increasing horizontal gas-pressure gradient between the interior of the granule and the region above the vortex tube. Directly above the vortex tube, the flow assumes transonic speeds and gas pressure and temperature have a local minimum. Since pressure and temperature are low, the opacity above the vortex tube is reduced (dip in the $\log\tau = -1$ surface), which opens a relatively transparent view to the cool interior of the vortex tube. This is the

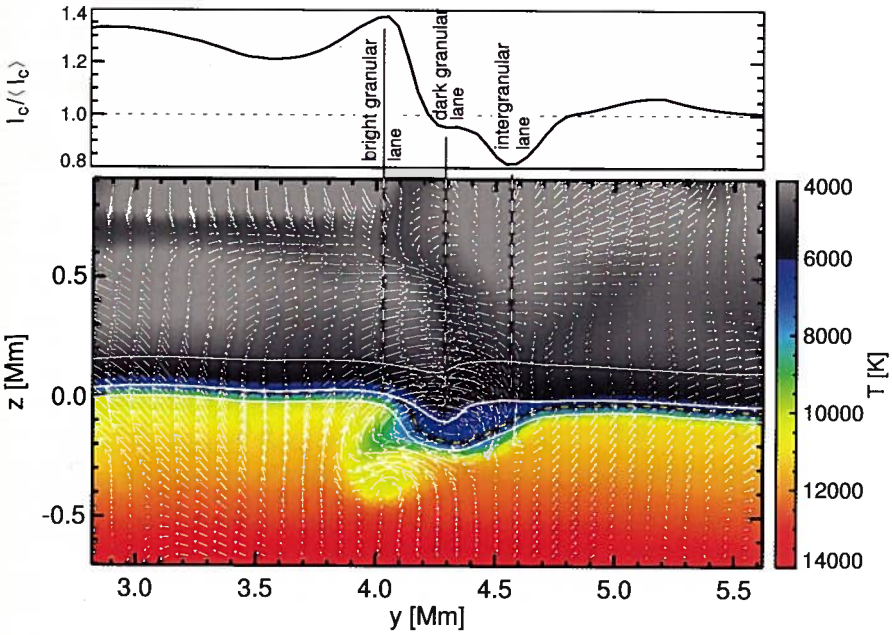

Figure 4. Vertical cross section through the computational domain for the event and at the location shown in Figure 3a. The top panel shows the emergent synthesized continuum intensity at $\lambda = 5250$ Å. Colors indicate temperature and the arrows indicate the velocity field. The white contours indicate optical depths of $\log \tau_c = -1$, 0, and 1, from top to bottom, respectively, the yellow/black dashed contour represents the 7000 K isotherm. The longest arrows correspond to a velocity of 8.5 km s^{-1}. From Steiner et al. (2010). Reproduced by permission of the AAS.

origin of the dark lane, which trails the bright granular lane. Further downstream, the horizontal wind decelerates and collides with flows from the neighboring granule. In some cases the intensity in this region increases again (but not in the case of Fig. 4) before the flow turns into the downdraft, which causes the dark intergranular lane at $x = 4.6$ Mm.

In most cases, the central axis of the vortex tube is relatively steady, staying close to but below the surface of $\tau_c = 1$. It is rather the shape and size of the vortex tube which changes in time and causes the horizontal displacement of the bright lane and the expansion of the trailing darkish area. Sometimes vortex tubes start with an oval cross section, with the major axis being oriented in the vertical direction and evolve into an oval, flat cross section with the major axis oriented in the horizontal direction. In particular, extended dark areas moving into granules (cf. Figs. 2f and 3f) are caused by strongly flattened vortex tubes, which start to resemble vortex sheets. It is remarkable that the downdraft side of the vortex tube hardly ever shows a deep downdraft. Rather, this downdraft is shallow and runs into the vortex flow, where it gets recycled and contributes to the growth of the vortex tube. However, this state of matter is hidden from the visible surface so that in the intensity map the location of the downdraft appears to be a normal intergranular lane (cf. Figure 3a). Without having carried out a systematic

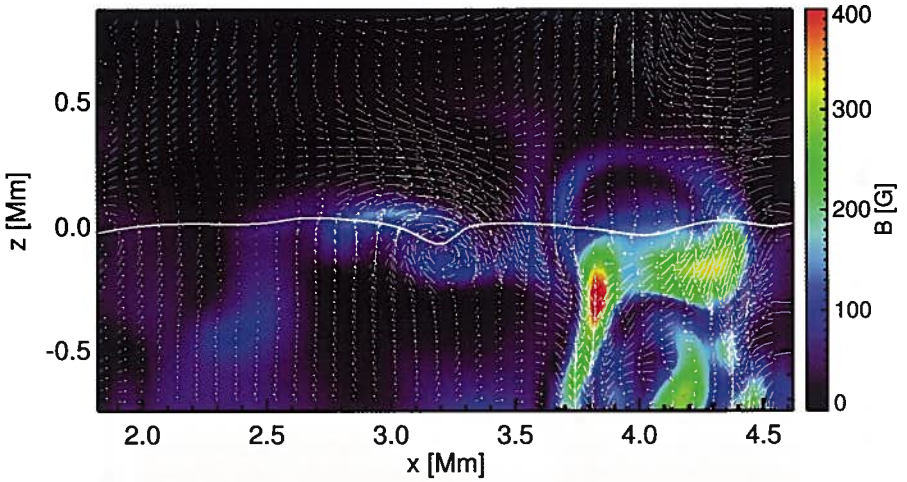

Figure 5. Vertical cross section through the computational domain. Colors represent the magnetic field strength and the arrows indicate the velocity field. The white contour indicates optical depths $\tau_c = 1$. A vortex tube is visible with the center located at $(x, z) = (3.2, -0.1)$ Mm. Above the vortex-tube, close to the $\tau_c = 1$ surface, horizontal magnetic field of a strength up to 150 G forms. Horizontal velocities reach there 6.5 km s^{-1}.

study yet, it seems that an initial, regular intergranular downdraft may get wrapped into a vortex tube in the course of a collision of two neighboring granules. This would explain the absence of deep downdrafts at the location of vortex tubes. This scenario is supported by the fact that usually a regular downdraft is present outside of both ends of the vortex tube.

The cores of closed stream lines in the vortex tubes have a typical mean radius of 150 km. Velocities along a stream line at this distance are typically 3 km s^{-1} on the lateral sides, 8 km s^{-1} on the top side, and 5 km s^{-1} on the bottom side. Thus, one revolution takes about half a minute, which is considerably shorter than the lifetime of typical vortex tubes.

Sometimes, the bright lane is missing, e.g., when the upflow has enough lateral space to escape from the vortex tube in the horizontal direction. In this case a solitary dark lane forms above the vortex-tube center. Sometimes a flat vortex tube stays at the surface of a granule having the appearance of a normal intergranular lanes, which, however, does not harbor a deep downdraft. Conspicuously bright, small granules are often the result of two neighboring vortex tubes with opposite sense of rotation.

In the simulation, we see occasional magnetic field intensification at locations of vortex tubes—a few cases rather show field expulsion. Whenever magnetic fields are present, they tend to point in the horizontal direction near or above the $\tau_c = 1$ surface. An example is given in Figure 5. Hence, vortex tubes might be a significant source of horizontal magnetic fields in the photosphere. Patches of horizontal fields are found to be preferentially located near the boundaries of granules (Ishikawa et al. 2010; Danilovic et al. 2010), which coincides with the location of vortex tubes. However, our

observations, which include the polarization signal, do not indicate enhanced magnetic fields at locations of granular lanes.

6. Conclusions

From observations with the imaging magnetograph IMaX on board the balloon-borne solar observatory SUNRISE, we find granular fine structure, consisting of moving lanes, which are usually composed of a leading bright rim and a trailing dark edge. They move from the border of a granule into the granule itself. Sometimes they retreat back again before they disappear. Although we have noticed these features for the first time in SUNRISE data, after completing the analysis we also looked at other data sets and found them there as well. In fact, latest time sequences from the 1.6 m New Solar Telescope of the Big Bear Solar Observatory show that most if not all granules show one ore more instances of granular lanes[1]. With the help of a numerical simulation of solar surface convection, we identify these objects as vortex tubes.

From the equation of vorticity ω for an inviscid, compressible medium,

$$\frac{\mathrm{D}\omega}{\mathrm{D}t} = \nabla(\boldsymbol{v}\cdot\boldsymbol{\omega}) + \frac{1}{\rho^2}\nabla\rho\times\nabla p\,, \tag{1}$$

one can see that the baroclinic term (second term on the right hand side) can be a source of vorticity. This term becomes important for non-isentropic flows, which indeed exist at the solar surface, where radiative transfer takes place. In particular, vorticity is generated near the boundaries of granules and in the intergranular downdrafts (Nordlund et al. 2009; Muthsam et al. 2010). The behavior of vorticity in a gravitationally stratified atmosphere was studied by Arendt (1993a,b). Since the gradients of pressure and density are close to vertical, their cross product is horizontal, which explains the horizontal orientation of the generated vorticity according to Equation 1. This generation is different from the generation of vortical flows by conservation of angular momentum. The latter mechanism is probably responsible for the vortical flows discovered by Bonet et al. (2008, 2010).

Vortex tubes are a fundamental structure element of turbulence (Frisch 1995; Davidson 2004), where they play a key role in transferring energy from large scales to the smallest, dissipative scales in the energy cascade. It is tempting to speculate that the vortex tubes discovered in the present investigation may represent just one stage in a similar energy cascade. They could potentially transport mechanical energy to different locations and scales. The size of the vortex tubes seen in this investigation is close to the spatial resolution limits of both the observation and the numerical simulation. It should therefore be rewarding to further push these limits to smaller scales, as the Sun seems to provide a unique opportunity for the study of vortex tubes in a profoundly stratified medium.

Acknowledgments. The German contribution to SUNRISE is funded by the Bundesministerium für Wirtschaft und Technologie through Deutsches Zentrum für Luft- und Raumfahrt e.V. (DLR), Grant No. 50 OU 0401, and by the Innovationsfond of the President of the Max Planck Society (MPG). The Spanish contribution has been funded

[1] see nst_tio_20100803.mpg at `http://www.bbso.njit.edu/gallery/`

by the Spanish MICINN under projects ESP2006-13030-C06 and AYA2009-14105-C06 (including European FEDER funds). The HAO contribution was partly funded through NASA grant NNX08AH38G. The National Center for Atmospheric Research (NCAR) is sponsored by the National Science Foundation. This work was supported by the WCU grant R31-10016 funded by the Korean Ministry of Education, Science, and Technology.

References

Arendt, S. 1993a, Geophysical and Astrophysical Fluid Dynamics, 68, 59
— 1993b, Geophysical and Astrophysical Fluid Dynamics, 70, 161
Barthol, P., Gandorfer, A., Solanki, S. K., Schüssler, M., Chares, B., Curdt, W., Deutsch, W., Feller, A., Germerott, D., Grauf, B., Heerlein, K., Hirzberger, J., Kolleck, M., Meller, R., Müller, R., Riethmüller, T. L., Tomasch, G., Knölker, M., Lites, B. W., Card, G., Elmore, D., Fox, J., Lecinski, A., Nelson, P., Summers, R., Watt, A., Martínez Pillet, V., Bonet, J. A., Schmidt, W., Berkefeld, T., Title, A. M., Domingo, V., Gasent Blesa, J. L., Del Toro Iniesta, J. C., López Jiménez, A., Álvarez-Herrero, A., Sabau-Graziati, L., Widani, C., Haberler, P., Härtel, K., Kampf, D., Levin, T., Pérez Grande, I., Sanz-Andrés, A., & Schmidt, E. 2011, Solar Phys., 268, 1
Berkefeld, T., Schmidt, W., Soltau, D., Bell, A., Doerr, H. P., Feger, B., Friedlein, R., Gerber, K., Heidecke, F., Kentischer, T., v. D. Lühe, O., Sigwarth, M., Wälde, E., Barthol, P., Deutsch, W., Gandorfer, A., Germerott, D., Grauf, B., Meller, R., Álvarez-Herrero, A., Knölker, M., Martínez Pillet, V., Solanki, S. K., & Title, A. M. 2011, Solar Phys., 268, 103
Bonet, J. A., Márquez, I., Sánchez Almeida, J., Cabello, I., & Domingo, V. 2008, ApJ, 687, L131
Bonet, J. A., Márquez, I., Sánchez Almeida, J., Palacios, J., Martínez Pillet, V., Solanki, S. K., del Toro Iniesta, J. C., Domingo, V., Berkefeld, T., Schmidt, W., Gandorfer, A., Barthol, P., & Knölker, M. 2010, ApJ, 723, L139
Davidson, P. A. 2004, Turbulence : An Introduction for Scientists and Engineers (Cambridge: Cambridge Univ. Press)
Danilovic, S., Beeck, B., Pietarila, A., Schüssler, M., Solanki, S. K., Martínez Pillet, V., Bonet, J. A., del Toro Iniesta, J. C., Domingo, V., Barthol, P., Berkefeld, T., Gandorfer, A., Knölker, M., Schmidt, W., & Title, A. M. 2010, ApJ, 723, L149
Freytag, B., Steffen, M., & Dorch, B. 2002, Astronomische Nachrichten, 323, 213
Freytag, B., Steffen, M., Ludwig, H.-G., Wedemeyer-Böhm, S., Schaffenberger, W., & Steiner, O. 2011, J. Comput. Phys., submitted
Frisch, U. 1995, Turbulence. The legacy of A. N. Kolmogorov. (Cambridge: Cambridge Univ. Press)
Ishikawa, R., Tsuneta, S., & Jurčák, J. 2010, ApJ, 713, 1310
Martínez Pillet, V., Del Toro Iniesta, J. C., Álvarez-Herrero, A., Domingo, V., Bonet, J. A., González Fernández, L., López Jiménez, A., Pastor, C., Gasent Blesa, J. L., Mellado, P., Piqueras, J., Aparicio, B., Balaguer, M., Ballesteros, E., Belenguer, T., Bellot Rubio, L. R., Berkefeld, T., Collados, M., Deutsch, W., Feller, A., Girela, F., Grauf, B., Heredero, R. L., Herranz, M., Jerónimo, J. M., Laguna, H., Meller, R., Menéndez, M., Morales, R., Orozco Suárez, D., Ramos, G., Reina, M., Ramos, J. L., Rodríguez, P., Sánchez, A., Uribe-Patarroyo, N., Barthol, P., Gandorfer, A., Knölker, M., Schmidt, W., Solanki, S. K., & Vargas Domínguez, S. 2011, Solar Phys., 268, 57
Muthsam, H. J., Kupka, F., Löw-Baselli, B., Obertscheider, C., Langer, M., & Lenz, P. 2010, New Astronomy, 15, 460
Nordlund, Å., Stein, R. F., & Asplund, M. 2009, Living Reviews in Solar Physics, 6, 2
Schaffenberger, W., Wedemeyer-Böhm, S., Steiner, O., & Freytag, B. 2005, in Chromospheric and Coronal Magnetic Fields, edited by D. E. Innes, A. Lagg, & S. A. Solanki (Noord-

wijk: ESA), vol. 596 of ESA Special Publication
— 2006, in Solar MHD Theory and Observations: A High Spatial Resolution Perspective, edited by J. Leibacher, R. F. Stein, & H. Uitenbroek, vol. 354 of ASP Conf. Ser., 345
Solanki, S. K., Barthol, P., Danilovic, S., Feller, A., Gandorfer, A., Hirzberger, J., Riethmüller, T. L., Schüssler, M., Bonet, J. A., Martínez Pillet, V., del Toro Iniesta, J. C., Domingo, V., Palacios, J., Knölker, M., Bello González, N., Berkefeld, T., Franz, M., Schmidt, W., & Title, A. M. 2010, ApJ, 723, L127
Steiner, O., Franz, M., Bello González, N., Nutto, C., Rezaei, R., Martínez Pillet, V., Bonet Navarro, J. A., del Toro Iniesta, J. C., Domingo, V., Solanki, S. K., Knölker, M., Schmidt, W., Barthol, P., & Gandorfer, A. 2010, ApJ, 723, L180
Steiner, O., Rezaei, R., Schaffenberger, W., & Wedemeyer-Böhm, S. 2008, ApJ, 680, L85
Stix, M. 2002, The Sun: An Introduction (Berlin: Springer), 2nd ed.